Jurnal Teknologi, 37(A) Dis. 2002: 1–22

AN ANALYSIS OF THE STATIC AND DYNAMIC STABILITY OF AN HYPERSONIC TRANSPORT AIRCRAFT LONGITUDINAL MOTION FLYING AT HYPERSONIC SPEEDS AND VARIOUS HEIGHTS

D. MCLEAN[1], Z.A. ZALUDIN[2] & P.R. ARORA[3]

Abstract. A study of the static and dynamic stability of an hypothetical hypersonic transport aircraft was conducted based on a mathematical model of the longitudinal motion of the aircraft flying at a number of different flight conditions. The result from the stability analysis has shown that the aircraft becomes even less stable at higher Mach numbers and heights than the nominal flight condition. Also discussed here is the scramjet engine condition when the aircraft was simulated to be flying at hypersonic speeds and different heights.

Keywords: aircraft dynamics, dynamic stability, static stability, scramjet engine

Abstrak. Suatu kajian tentang kestabilan statik dan dinamik pesawat pengangkutan hipersonik hipotesis telah dilakukan dengan menggunakan model matematik untuk pergerakan membujur semasa penerbangan di keadaan penerbangan yang berlainan. Hasil daripada analisis kestabilan menunjukkan bahawa pesawat tersebut akan menjadi lebih tidak stabil apabila penerbangan di nombor Mach dan ketinggian yang lebih tinggi daripada keadaan penerbangan nominal. Juga disertakan di sini keadaan enjin scramjet apabila pesawat ini terbang pada kelajuan hipersonik dan ketinggian yang berlainan.

Kata Kunci: dinamik pesawat, kestabilan dinamik, kestabilan statik, enjin scramjet

List of Symbols

δ_F – flap surface deflection;
A_D – ratio of engine diffuser area;
T_o – temperature across the engine combustor (°R);
δ_A – aileron deflection (rad)
δ_R – rudder deflection (rad)
τ_1 – Vehicle nose angle from side view (rad)
τ_2 – Vehicle tail angle from side view (rad)
L – Vehicle length (ft)
L_1 – Distance from vehicle nose to apex (ft)
L_2 – Distance from vehicle tail to apex (ft)

[1] Professor, Department of Aeronautics and Astronautics, Southampton University, Southampton, UK.
[2&3] Research Scientists, Department of Aerospace Engineering, Universiti Putra Malaysia, Serdang, Malaysia.

l_1 – lower fore-body surface length, $L_1/\cos\ \tau_1$
l_2 – lower aft-body surface length, $L_2/\cos\ \tau_2$
h – vehicle height from ground (ft)
$\bar{x}$ – x-distance to vehicle mass centre (ft)
$\bar{z}$ – z-distance to vehicle mass centre (ft)
x_{cs} – control surface position relative to the vehicle's mass centre (ft) in x-axis direction
z_{cs} – control surface position relative to the vehicle's mass centre (ft) in z-axis direction
δ_o – trimmed flap deflection (rad)
x – Body Axis x-direction
z – Body Axis z-direction
I_{yy} – inertia per unit width about the Y-axis,
S_{cs} – control surface reference area,
ω_1 – frequency of the first in-vacuo vibration mode
ζ_1 – damping ratio of first in-vacuo vibration mode
m – vehicle mass per unit width (lb/ft)
m – generalised elastic mass per unit width (lb/ft).
M_∞ – Mach number at freestream condition
M_1 – Mach number at the engine diffuser inlet
M_2 – Mach number at the engine combustor inlet
M_3 – Mach number at the engine internal nozzle inlet
M_e – Mach number at the engine internal nozzle exit
P_∞ – Pressure at freestream condition (lb/ft^2)
P_1 – Pressure at the engine diffuser inlet (lb/ft^2)
P_2 – Pressure at the engine combustor inlet (lb/ft^2)
P_3 – Pressure at the engine internal nozzle inlet (lb/ft^2)
P_e – Pressure at the engine internal nozzle exit (lb/ft^2)
q – Pitch rate (rad/s)
q_∞ – dynamic pressure (lb/ft^2)
S_{cs} – Control surface reference area (ft^2)
S – Wing reference area (includes area projected to fuselage centreline) (ft^2)
T_o – Total temperature across combustor (°R)
T_∞ – Temperature at freestream condition (°R)
T_1 – Temperature at the engine diffuser inlet (°R)
T_2 – Temperature at the engine combustor inlet (°R)
T_3 – Temperature at the engine internal nozzle inlet (°R)
T_e – Temperature at the engine internal nozzle exit (°R)
a_∞ – Speed of sound (ft/s)
γ – specific heat capacity

Δ – perturbation from equilibrium flight condition
C_{PN} – Pressure coefficient
θ_L – local flow deflection angle (rad)

1.0 INTRODUCTION

It is expected that in the future Hypersonic Transport (HST) aircraft will provide fast long-haul passenger flights. The ability of such aircraft to carry between 200 – 300 passengers flying at hypersonic speeds between continents has provided aeronautical designers with an incentive to tackle some of the greatest challenges involved in the history of aviation. The existence of such HST aircraft could significantly change the nature of long distance flight. A lack of detailed understanding at present of the actual behaviour of an HST aircraft flying at hypersonic speeds has led aeronautical engineers to construct mathematical models to simulate the aircraft when it is subjected to disturbances or commanded control inputs.

It is especially important in the early design stages of an automatic flight control system for a new aircraft such as the Hypersonic Transport (HST) aircraft to analyse the condition affecting the aircraft's dynamic behaviour. It is through this basic approach that critical configuration-dependent dynamics-and-control issues can be identified as well as the development of a basic understanding of the physical genesis of these control issues. The stability condition of the longitudinal motion of the HST aircraft flying at various hypersonic speeds and at different altitudes is addressed in this paper.

2.0 THE FLIGHT MISSION

The primary mission considered is the transportation of passengers from one continent to another. The phases of flight considered are as follows: flight at subsonic speeds and low supersonic speeds using turbojet engine; the next flight phase is carried out at moderate supersonic speeds up to low hypersonic speeds for which a ramjet/turbo ramjet engine is used. At about Mach 5.0, a scramjet engine is activated which must be operated at high dynamic pressure to obtain the maximum propulsive efficiency. However, since aerodynamic heating and drag also increase with dynamic pressure, the benefits of high propulsive efficiency have to be balanced against temperature and structural constraints. However, this issue is beyond the scope of the work presented here.

In the study of aircraft flying at hypersonic speeds using air-breathing engines, the region at which least is known [1] is when the aircraft is flying with the scramjet engine activated. The scramjet-phase is of special interest because it is critical if airbreathing propulsion is to have promise for this mission. The investigation of the dynamics of the aircraft presented here focuses on the scramjet-powered phase of flight. The operating principles of a scramjet are the same as those for a ramjet except that com-

bustion takes place at supersonic speeds. The scramjet engine has the highest performance (as measured by specific impulse) in the hypersonic speed regime [2].

3.0 THE PROBLEM

In the absence of any flight data, there is considerable uncertainty about the nature of the motion of the HST aircraft flying at hypersonic speeds and at the altitudes the aircraft needs to fly when the scramjet engine is active. To overcome this uncertainty, a mathematical model of the aircraft dynamics is commonly used to simulate the aircraft responses when the aircraft is subjected to disturbances and commanded inputs. There are only few published mathematical model on HST aircraft because general access to them is restricted. In 1989, the National Aeronautics and Space Administration (NASA) published for general academic use the first mathematical model of an hypersonic aircraft which was named Generic Hypersonic Aerodynamic Model Example, GHAME [3]. The model was developed by NASA to provide universities and USA government agencies with an unclassified model of a single-stage-to-orbit (SSTO) vehicle. GHAME was limited to one flight condition at Mach 6.0 and at a height of 60 000 ft. The sources of force and moment were assumed to be contributed solely by the aircraft aerodynamics and its engines, but later research [4-6] reported that aircraft aeroelastic effects also needed to be considered since the aircraft propulsion system was extremely sensitive to changes in angle of attack and in dynamic pressure. There are also other mathematical models of hypersonic aircraft published [7-9] but these models seemed inadequate for the type of stability analysis at various flight condition which are presented here. It was also found that the mathematical models proposed by these authors did not include details of derivation and nor any aeroelastic effects of the aircraft structure was taken into account.

Chavez and Schmidt [10] published an extended and unclassified mathematical model of a single-stage-to-orbit (SSTO) hypersonic aircraft. It was the most comprehensive mathematical model available at the time and remains useful today. In that model, three sources of force and moment were considered; aerodynamics, propulsion system and aeroelastic effects.

4.0 THE VEHICLE

For convenience of reference, the name **HYPERION** has been given by the present authors to this mathematical model of the dynamic motion of the hypersonic transport aircraft. A sketch of this hypothetical aircraft is shown in Figure 1.

The mathematical model is linear and has five control inputs, δ_F, A_D, T_o, δ_A and δ_R. The first three controls are used for controlling longitudinal motion and the final two are used for controlling the aircraft lateral motion. Chavez and Schmidt [10] based the analysis of the mathematical model of the hypersonic aircraft on a two dimensional representation which is shown as Figure 2.

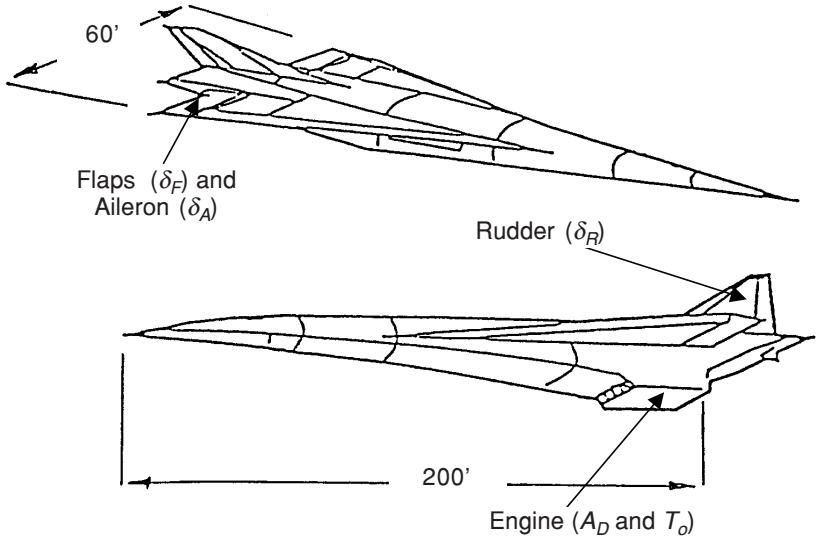

Figure 1 The Generic Hypersonic aircraft sketch

By using this two-dimensional model, two important features simplify the analysis of the dynamic characteristics of the aircraft; a forebody compression surface and an

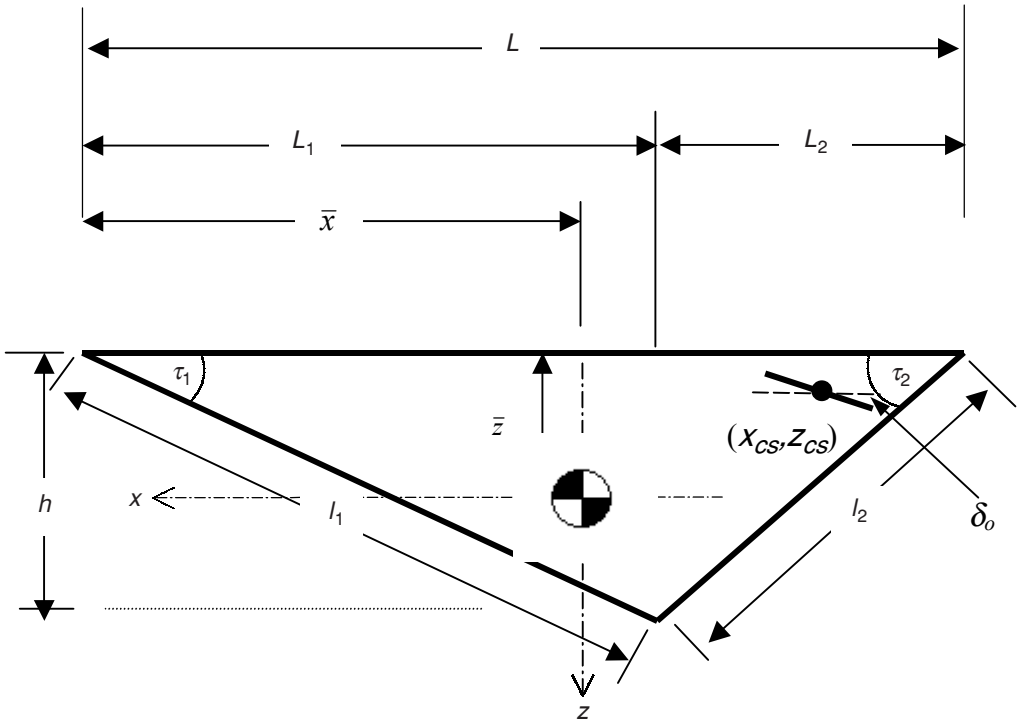

Figure 2 Two dimensional representation and geometrical details of the HST vehicle

afterbody/nozzle expansion surface. The lower forebody compression surface serves as a lifter and acts as an external diffuser for the engine. The vehicle afterbody and nozzle surfaces serve as external expansion nozzles which produce both thrust and lift. The aircraft geometry data [10] used for all the mathematical models of the longitudinal motion considered in this paper is shown is Table 1. The elastic motion of the vehicle was characterised by a single structural bending mode. It is represented in Figure 3 as a change in the effective slope of the lower fore- and afterbody surfaces.

Table 1 Aircraft geometry data

AIRCRAFT GEOMETRY					
τ_1	=	0.24435 rad (14°)	δ_o	=	0.52395 rad (30.02°)
τ_2	=	0.34907 rad (20°)	h	=	22.20 ft
L	=	150 ft	$\Delta\tau_1$	=	1.7453×10^{-2} rad (1°)
L_1	=	89.02 ft	$\Delta\tau_2$	=	1.7453×10^{-2} rad (1°)
L_2	=	60.98 ft	m	=	500 slug/ft
$\frac{S_{cs}}{b}$	=	22.5 ft	m	=	40 slug/ft
$\bar{x}$	=	90.00 ft	g	=	32.2 ft/s^2
$\bar{z}$	=	11.25 ft	I_{yy}	=	1.0×10^6 slug ft^2/ft
x_{cs}	=	–52.50 ft	ω_1	=	18 rad/s
z_{cs}	=	–11.25 ft	ζ_1	=	0.02
l_1	=	91.756 ft	l_2	=	64.894 ft

The characterisation of the elastic motion of the vehicle is kept simple to aid the analysis whilst still retaining first-order effects.

Since the HST was assumed to be propelled by a scramjet engine, the dynamics of the engine were assumed to be contained within a module consisting of three main

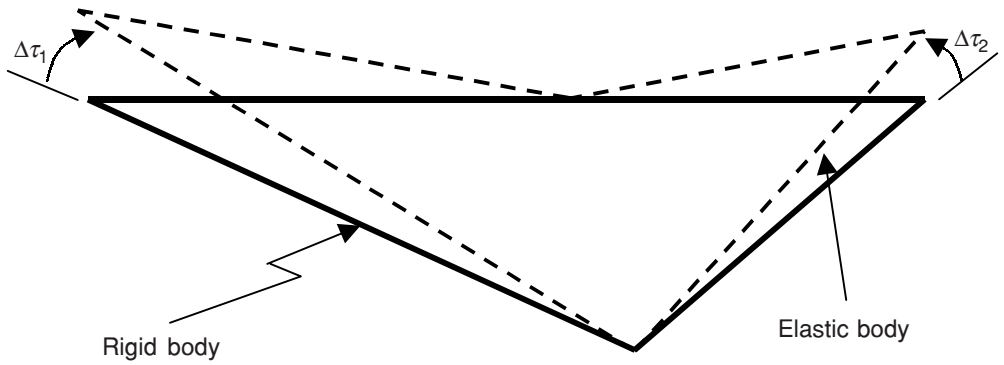

Figure 3 Elastic vehicle model

sections: a supersonic diffuser, a supersonic combustor and an internal supersonic expansion nozzle. The two dimensional representation of the engine is shown in Figure 4. Points on the engine have been marked to indicate the diffuser inlet, combustor inlet, combustor exit and nozzle exit. The inlet conditions to the engine were determined by the aerodynamics associated with the lower forebody surface of the vehicle, whereas the exit conditions of the engine were strongly affected by the vehicle's afterbody/nozzle surfaces. The engine was considered to have a variable diffuser area ratio. The atmospheric conditions corresponding to the various flight conditions in

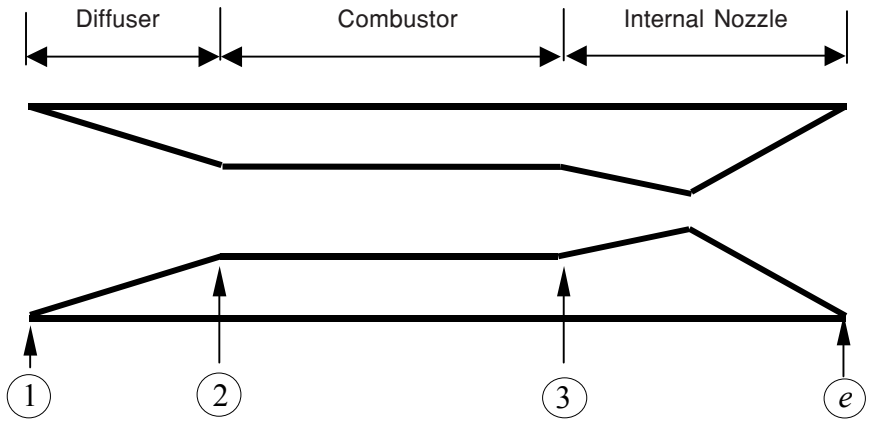

Figure 4 Scramjet engine module and sections

the analysis of the aircraft dynamics are listed Table 2. These data were obtained from Rogers and Mayhew [11].

Table 2 Flight condition data

Height (ft)	P_∞(lb/ft^2)	T_∞(°R)	a_∞(ft/s)	γ
80 000	58.938	397.74	977.6	1.4007323
85 000	46.461	400.34	981.09	1.4007207
90 000	37.152	403.08	984.40	1.4007085
95 000	29.574	405.82	987.65	1.4006964
100 000	23.406	408.56	990.9	1.4006841

5.0 ENGINE CONDITIONS FOR AIRCRAFT MODELS FLYING AT VARIOUS HYPERSONIC SPEEDS AND HEIGHTS

For the HST aircraft to fly at hypersonic speeds, it is known that a scramjet engine must be used and activated at approximately Mach 5.0, to obtain the maximum pro-

pulsive efficiency. However, little is known of the conditions of the scramjet engine when the aircraft is flying at any flight condition [1]. Presented next are the conditions of the scramjet engine at various hypersonic speeds and height obtained for the stability analysis.

The equations needed to calculate the engine condition data can be found from Chavez and Schmidt [10], but have been included in this section for the reader's convenience. The Mach number, pressure and temperature at a point 1 of the scramjet jet engine [see Figure 4] were found using the following equations. Subscripts represent the position on the engine where the condition was calculated.

$$M_1 = \frac{M_\infty \cos\theta_L}{\sqrt{(1+\frac{1}{2}\gamma-1)M_\infty^2 \sin^2\theta_L}} \tag{1}$$

$$P_1 = P_\infty\left[1+\frac{1}{2}\gamma M_\infty^2 C_{PN}\sin^2\theta_L\right] \tag{2}$$

$$T_1 = T_\infty\left[1+\frac{1}{2}(\gamma-1)M_\infty^2\sin^2\theta_L\right] \tag{3}$$

For the diffuser,

$$\frac{\left[1+\frac{1}{2}(\gamma-1)M_2^2\right]^{(\gamma+1)/(\gamma-1)}}{M_2^2} = (\bar{A}_D)^2\frac{\left[1+\frac{1}{2}(\gamma-1)M_1^2\right]^{(\gamma+1)/(\gamma-1)}}{M_1^2} \tag{4}$$

$$P_2 = P_1\left[\frac{1+\frac{1}{2}(\gamma-1)M_1^2}{1+\frac{1}{2}(\gamma-1)M_2^2}\right]^{\gamma/(\gamma-1)} \tag{5}$$

$$T_2 = T_1\left[\frac{1+\frac{1}{2}(\gamma-1)M_1^2}{1+\frac{1}{2}(\gamma-1)M_2^2}\right] \tag{6}$$

For the combustor,

$$\frac{M_3^2\left[1+\frac{1}{2}(\gamma-1)M_3^2\right]}{\left(\gamma M_3^2+1\right)^2} = \frac{M_2^2\left(1+\frac{1}{2}(\gamma-1)M_2^2\right)}{\left(\gamma M_2^2+1\right)^2} + \frac{M_2^2}{\left(\gamma M_2^2+1\right)^2}\left[\frac{T_o}{T_2}\right] \tag{7}$$

$$P_3 = P_2\left(\frac{1+\gamma M_2^2}{1+\gamma M_3^2}\right) \tag{8}$$

$$T_3 = T_2\left[\left(\frac{1+\gamma M_2^2}{1+\gamma M_3^2}\right)\left(\frac{M_3}{M_2}\right)\right]^2 \tag{9}$$

M_3, P_3 and T_3 are the combustor exit/internal nozzle inlet static conditions. T_o is the increase in total temperature across the combustor due to combustion of the fuel. For the internal nozzle,

$$\frac{\left[1+\frac{1}{2}(\gamma-1)M_e^2\right]^{(\gamma+1)/(\gamma-1)}}{M_e^2} = \left(\bar{A}_N\right)^2 \frac{\left[1+\frac{1}{2}(\gamma-1)M_3^2\right]^{(\gamma+1)/(\gamma-1)}}{M_3^2} \tag{10}$$

$$P_e = P_3\left[\frac{1+\frac{1}{2}(\gamma-1)M_3^2}{1+\frac{1}{2}(\gamma-1)M_e^2}\right]^{\gamma/(\gamma-1)} \tag{11}$$

$$T_e = T_3\left[\frac{1+\frac{1}{2}(\gamma-1)M_3^2}{1+\frac{1}{2}(\gamma-1)M_e^2}\right] \tag{12}$$

M_e, P_e and T_e are the internal nozzle/engine exit (static) conditions. $\bar{A}_N$ is the internal nozzle ratio, defined as the ratio of the nozzle exit area to nozzle inlet area.

One method of solving Eqns. (4), (7) and (10) to obtain the values M_2, M_3 and M_e respectively is to use interpolation. Let Eqn. (4) be written as:

$$\frac{\left[1+\frac{1}{2}(\gamma-1)M_2^2\right]^{(\gamma+1)/(\gamma-1)}}{M_2^2} = (\bar{A}_D)^2 \frac{\left[1+\frac{1}{2}(\gamma-1)M_1^2\right]^{(\gamma+1)/(\gamma-1)}}{M_1^2} \tag{13}$$

Then, a graph of y versus M_2 can be plotted. The value of M_2 at the flight condition being considered is the value of M_2 in the graph where the curve cuts the x-axis. Substituting this value into Eqns. (5) and (6) allows P_2 and T_2 to be evaluated.

Using these equations, the dynamic conditions of the aircraft model engine were calculated and tabulated. Table 3 presents data relating to the engine condition when the vehicle is flying at 85 000 ft at speeds from Mach 8 to Mach 15. Table 4 presents data relating to engine condition when the altitude of the vehicle changed with constant Mach number, Mach 8.

Table 3 Engine conditions at various Mach number flying at 85 000 ft

M_∞	8	9	10	11	12	13	14	15
M_1	6.2766	6.7488	7.1604	7.5185	7.8301	8.1013	8.3377	8.5443
M_2	3.8689	4.2258	4.5322	4.7958	5.0231	5.2194	5.3909	5.5400
M_3	1.9158	2.2475	2.5446	2.8155	3.0662	3.2988	3.4523	3.7173
M_e	3.9249	4.2456	4.5651	4.8752	5.1738	5.4602	5.6530	5.9908
P_∞	4.6461×10^{1}	4.6461×10^{1}	4.6461×10^{1}	4.6461×10^{1}	4.6461×10^{1}	4.6461×10^{1}	4.6461×10^{1}	4.6461×10^{1}
P_1	2.2650×10^{2}	2.7433×10^{2}	3.2778×10^{2}	3.8686×10^{2}	4.5156×10^{2}	5.2189×10^{2}	5.9784×10^{2}	6.7943×10^{2}
P_2	3.7017×10^{3}	4.3991×10^{3}	5.1881×10^{3}	6.0675×10^{3}	7.0363×10^{3}	8.0959×10^{3}	9.2309×10^{3}	1.0454×10^{4}
P_3	1.3241×10^{4}	1.4171×10^{4}	1.5339×10^{4}	1.6651×10^{4}	1.8048×10^{4}	1.9518×10^{4}	2.1758×10^{4}	2.2592×10^{4}
P_e	6.6333×10^{2}	7.8038×10^{2}	8.9707×10^{2}	1.0151×10^{3}	1.1348×10^{3}	1.2547×10^{3}	1.4160×10^{3}	1.4978×10^{3}
T_∞	4.0034×10^{2}	4.0034×10^{2}	4.0034×10^{2}	4.0034×10^{2}	4.0034×10^{2}	4.0034×10^{2}	4.0034×10^{2}	4.0034×10^{2}
T_1	6.2226×10^{2}	6.8120×10^{2}	7.4708×10^{2}	8.1990×10^{2}	8.9965×10^{2}	9.8633×10^{2}	1.0799×10^{3}	1.1805×10^{3}
T_2	1.3838×10^{3}	1.5067×10^{3}	1.6463×10^{3}	1.8020×10^{3}	1.9736×10^{3}	2.1610×10^{3}	2.3630×10^{3}	2.5804×10^{3}
T_3	4.3415×10^{3}	4.4225×10^{3}	4.5364×10^{3}	4.6775×10^{3}	4.8380×10^{3}	5.0172×10^{3}	5.3841×10^{3}	5.4259×10^{3}
T_e	1.8437×10^{3}	1.9296×10^{3}	2.0136×10^{3}	2.1011×10^{3}	2.1925×10^{3}	2.2882×10^{3}	2.4641×10^{3}	2.4965×10^{3}

Table 4 Engine conditions when the model was simulated flying at Mach 8. The heights at which the model was simulated flying were 80 000 ft, 85 000 ft, 90 000 ft, 95 000 ft and 100 000 ft.

Height	80 000	85 000	90 000	95 000	100 000
M_∞	8	8	8	8	8
M_1	6.2766	6.2766	6.2766	6.2766	6.2766
M_2	3.8689	3.8689	3.8689	3.8689	3.8689
M_3	1.9093	1.9158	1.9230	1.9297	1.9365
M_e	3.9192	3.9249	3.9313	3.9374	3.9435
P_∞	5.8938×10^{1}	4.6461×10^{1}	3.7152×10^{1}	2.9574×10^{1}	2.3406×10^{1}
P_1	2.8733×10^{2}	2.2650×10^{2}	1.8112×10^{2}	1.4418×10^{2}	1.1411×10^{2}
P_2	4.6954×10^{3}	3.7017×10^{3}	2.9602×10^{3}	2.3566×10^{3}	1.8652×10^{3}
P_3	1.6891×10^{4}	1.3241×10^{4}	1.0522×10^{4}	8.3279×10^{3}	6.5527×10^{3}
P_e	8.4423×10^{2}	6.6333×10^{2}	5.2846×10^{2}	4.1915×10^{2}	3.3056×10^{2}
T_∞	3.9774×10^{2}	4.0034×10^{2}	4.0308×10^{2}	4.0582×10^{2}	4.0856×10^{2}
T_1	6.1822×10^{2}	6.2226×10^{2}	6.2650×10^{2}	6.3075×10^{2}	6.3501×10^{2}
T_2	1.3748×10^{3}	1.3838×10^{3}	1.3933×10^{3}	1.4027×10^{3}	1.4122×10^{3}
T_3	4.3331×10^{3}	4.3415×10^{3}	4.3491×10^{3}	4.3580×10^{3}	4.3665×10^{3}
T_e	1.8388×10^{3}	1.8437×10^{3}	1.8482×10^{3}	1.8532×10^{3}	1.8581×10^{3}

The variation of the engine condition may be plotted for changes in speed and height to obtain an approximation for the values of Mach number, pressure and temperature for speeds and heights lying between those already considered. Four examples have been shown as Figures 5, 6, 7 and 8. The relationships between the conditions and speeds were found to be approximately linear. Refer to Figure 4 for the positions in the engine.

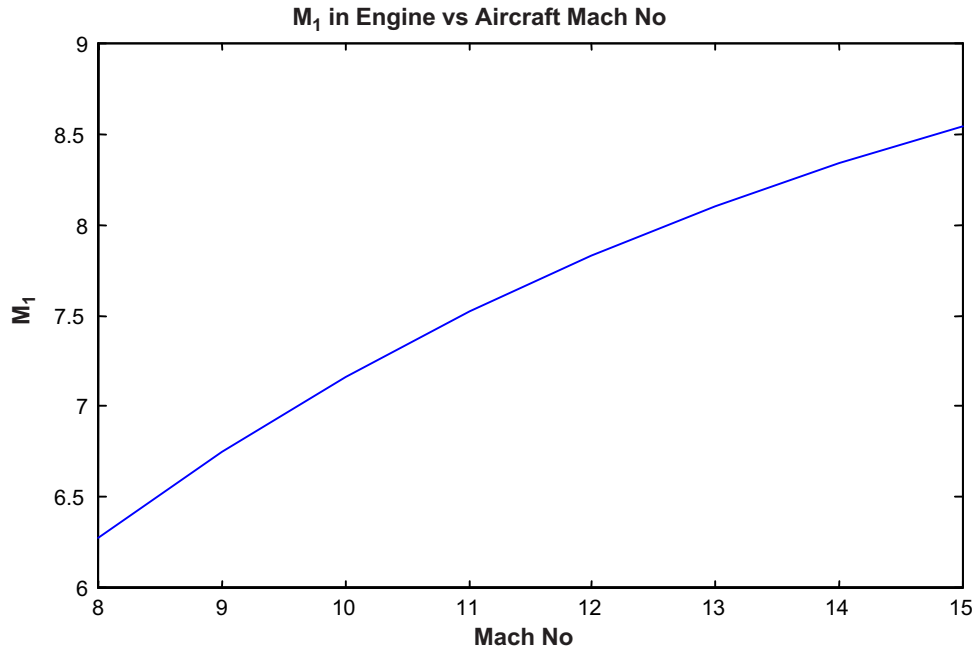

Figure 5 Mach number at station 1 of the scramjet engine when aircraft is flying at various Mach number.

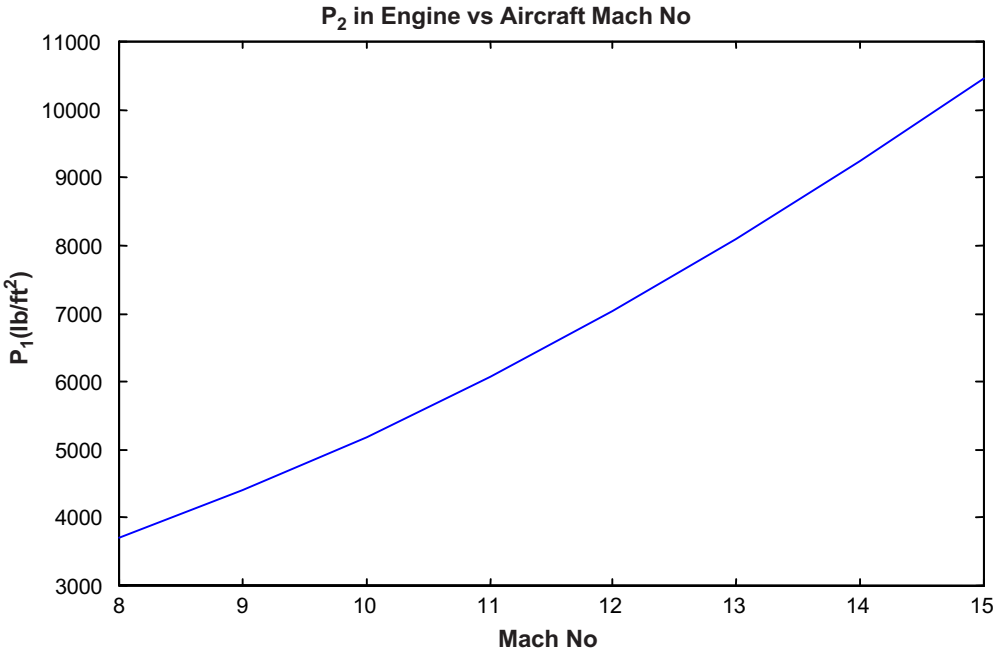

Figure 6 Pressure at station 2 of the scramjet engine when aircraft is flying at various Mach numbers.

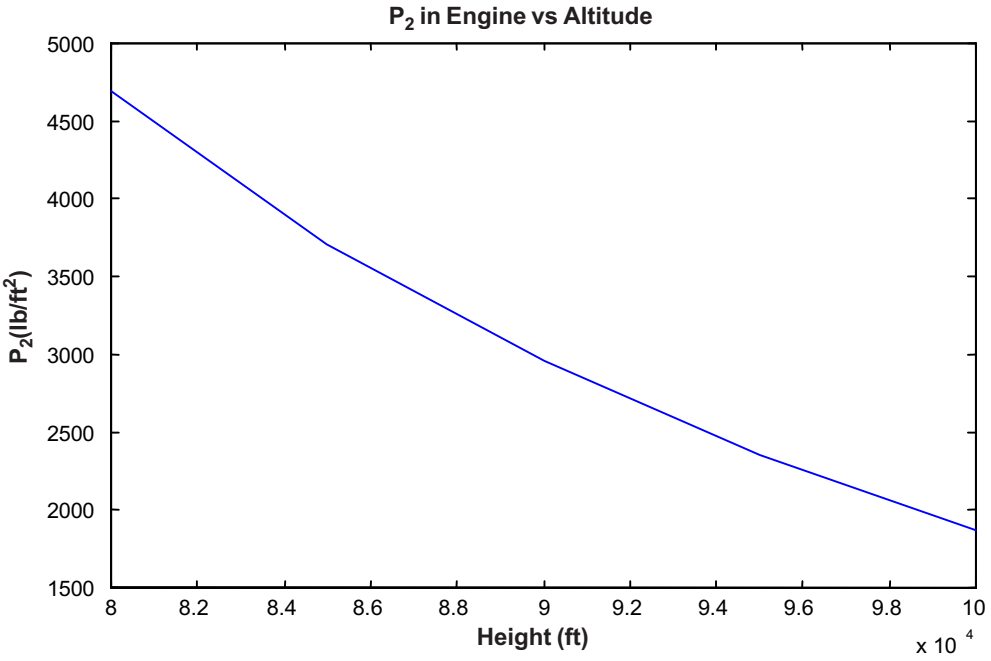

Figure 7 Pressure at station 2 of the scramjet engine when aircraft is flying at different altitudes

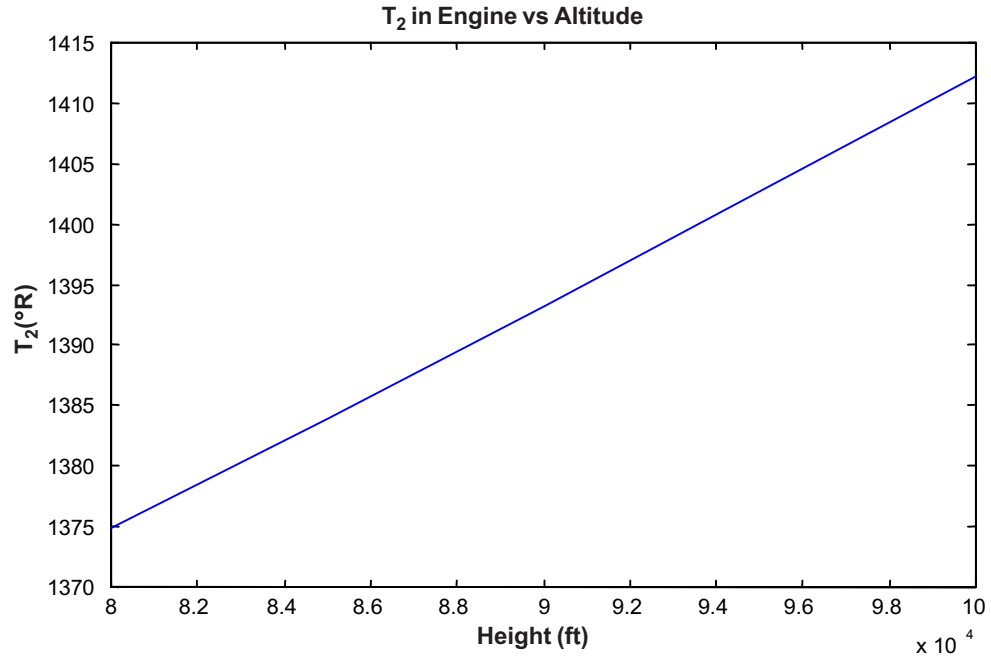

Figure 8 Temperature at station 2 of the scramjet engine when aircraft is flying at different altitudes

6.0 LONGITUDINAL MOTION OF AN HYPERSONIC TRANSPORT AIRCRAFT

The mathematical model of longitudinal motion used in this work was developed from an initial model based on that developed by Chavez and Schmidt [10]. Basically, the integrated modelling approach was used whereby contributing vector components (from three main sources; aerodynamic, propulsion and aeroelastic effects) were added to represent the forces in the X-axis direction, and the Z-axis direction and the total moment, M, about the centre of mass of the aircraft. A set of stability and control derivatives resulted from this analysis.

In the work reported here, the model of Chavez and Schmidt [10] had to be modified to permit the investigation of the dynamic stability of the aircraft at Mach numbers above 8.0 and at heights above 80 000 ft i.e during the scramjet-phase of the flight mission. Detailed analysis of the modification is documented in Zaludin [12]. The mathematical model used in the work was represented by a linear, time-invariant, state equation:

$$\dot{\mathbf{x}} = \mathbf{A}\mathbf{x} + \mathbf{B}\mathbf{u} \tag{14}$$

$\mathbf{x} \in \mathrm{R}^n$ represents the state vector and $\mathbf{u} \in \mathrm{R}^m$ represents the control vector. $\mathbf{A}$ is the state coefficient matrix and $\mathbf{B}$ is the driving matrix, of order $(n \times n)$ and $(n \times m)$ respectively. The state and the control variables are defined as

$$\mathbf{x} = \begin{bmatrix} \Delta u \ (\text{ft/s}) \\ \Delta \alpha \ (\text{rad}) \\ \Delta q \ (\text{rad/s}) \\ \Delta \theta \ (\text{rad}) \\ \Delta h \ (\text{ft}) \\ \Delta \eta \ (\text{rad}) \\ \Delta \dot{\eta} \ (\text{rad/s}) \end{bmatrix} \tag{15}$$

$$\mathbf{u} = \begin{bmatrix} \Delta \delta_F \ (\text{rad}) \\ \Delta A_D \\ \Delta T_o \ (^{\circ}\text{R}) \end{bmatrix} \tag{16}$$

The state variables are the forward speed u, the angle of attack α, the rate of change of the pitch attitude q, the pitch attitude θ, the height h, the bending displacement η and the rate of change of bending displacement η. The control variables are the flap δ_F,

the engine duct area A_d and the engine temperature across combustor T_0. The variables are all perturbations from an equilibrium flight condition. A complete set of formulae and data relating to flight and engine conditions, stability and control derivatives and the coefficients of state equations of the models at those flight conditions can be found in Chavez and Schmidt [10]. Shown below is an example of the matrices **A** and **B** obtained for the aircraft flying at Mach 8.0 and at an altitude of 90 000 ft.

A =

$$\begin{bmatrix} -3.3471\times10^{-3} & -2.8554\times10^{1} & 3.4022\times10^{-1} & -3.2200\times10^{1} & 6.4579\times10^{-4} & 1.4327\times10^{1} & 3.4273\times10^{-1} \\ -1.8392\times10^{-6} & -4.6796\times10^{-2} & 1.0002 & 0 & 3.5486\times10^{-7} & -3.1509\times10^{-2} & 1.7453\times10^{-4} \\ -7.6069\times10^{-6} & 3.4696 & -4.6131\times10^{-2} & 0 & 1.4677\times10^{-6} & 5.8332 & -4.2115\times10^{-2} \\ 0 & 0 & 1.0000 & 0 & 0 & 0 & 0 \\ 0 & -7.8752\times10^{3} & 0 & 7.8752\times10^{3} & 0 & 0 & 0 \\ 0 & 0 & 0 & 0 & 0 & 0 & 1.0000 \\ 1.1905\times10^{-3} & 4.3944\times10^{1} & -3.3322\times10^{-1} & 0 & -2.2970\times10^{-4} & -2.8006\times10^{2} & -1.0499 \end{bmatrix}$$

B =

$$\begin{bmatrix} -9.0831\times10^{1} & -1.3631\times10^{2} & 1.0589\times10^{-2} \\ -1.1566\times10^{-2} & 3.8048\times10^{-3} & -1.3311\times10^{-7} \\ -1.8801 & -6.5739\times10^{-1} & 5.4865\times10^{-5} \\ 0 & 0 & 0 \\ 0 & 0 & 0 \\ 0 & 0 & 0 \\ 0 & -7.8756\times10^{-1} & 2.7553\times10^{-5} \end{bmatrix}$$

The mathematical models of the longitudinal motion developed for this work was separated into two sets: the first consisted of models corresponding to the aircraft flying at a height of 85 000 ft and over a speed range from Mach 8.0 to Mach 15.0 in increment of 1.0 Mach. The second set consisted of models of the aircraft flying at a constant speed of Mach 8.0, but at heights of 80 000 to 100 000 ft in steps of 5000 ft. To aid the stability analysis, the state and control coefficient matrices, **A** and **B** were derived for each flight condition.

7.0 DYNAMIC STABILITY ANALYSIS

The dynamic stability of the aircraft corresponding to the mathematical model was investigated by examining the eigenvalues of the corresponding coefficient matrix, **A**, of the state-space equation [13]. The eigenvalues, γ, of the aircraft without any stability augmentation were the roots of the characteristics equation:

$$\det[\gamma\mathbf{I} - \mathbf{A}] = 0 \tag{17}$$

where I is an identity matrix. Any aircraft will be dynamically unstable if any of its eigenvalues has a positive real part. In this paper, the dynamic stability of the uncon-

trolled aircraft for the longitudinal motion has also been represented graphically in the form of eigenvalue diagrams. Tables 5 and 6 listed the eigenvalues of Hyperion flying at different speeds and heights.

From Tables 5 and 6, the short-period motion at all flight conditions considered appears to be unstable because one of the roots is a positive real number. The instabil-

Table 5 Eigenvalues of Hyperion Flying at Different Speeds and at a height of 85 000 ft

NATURAL MODES OF THE AIRCRAFT				
Mach No.	**Phugoid**	**Short Period**	**Structural Bending**	**Height**
8.0	$\lambda_{1,2} = -1.89 \times 10^{-3} \pm j5.78 \times 10^{-2}$	$\lambda_3 = 2.33$ $\lambda_4 = -2.49$	$\lambda_{5,6} = -5.50 \times 10^{-1} \pm j1.64 \times 10^{1}$	$\lambda_7 \to 0$
9.0	$\lambda_{1,2} = -2.39 \times 10^{-3} \pm j6.03 \times 10^{-2}$	$\lambda_3 = 2.70$ $\lambda_4 = -2.88$	$\lambda_{5,6} = -5.66 \times 10^{-1} \pm j1.60 \times 10^{1}$	$\lambda_7 \to 0$
10.0	$\lambda_{1,2} = -2.89 \times 10^{-3} \pm j6.26 \times 10^{-2}$	$\lambda_3 = -3.33$ $\lambda_4 = 3.10$	$\lambda_{5,6} = -5.79 \times 10^{-1} \pm j1.56 \times 10^{1}$	$\lambda_7 \to 0$
11.0	$\lambda_{1,2} = -3.33 \times 10^{-3} \pm j6.46 \times 10^{-2}$	$\lambda_3 = 3.56$ $\lambda_4 = -3.83$	$\lambda_{5,6} = -5.88 \times 10^{-1} \pm j1.50 \times 10^{1}$	$\lambda_7 \to 0$
12.0	$\lambda_{1,2} = -3.68 \times 10^{-3} \pm j6.62 \times 10^{-2}$	$\lambda_3 = 4.07$ $\lambda_4 = -4.41$	$\lambda_{5,6} = -5.89 \times 10^{-1} \pm j1.45 \times 10^{1}$	$\lambda_7 \to 0$
13.0	$\lambda_{1,2} = -4.03 \times 10^{-3} \pm j6.75 \times 10^{-2}$	$\lambda_3 = 4.65$ $\lambda_4 = -5.07$	$\lambda_{5,6} = -5.81 \times 10^{-1} \pm j1.39 \times 10^{1}$	$\lambda_7 \to 0$
14.0	$\lambda_{1,2} = -4.21 \times 10^{-3} \pm j6.86 \times 10^{-2}$	$\lambda_3 = 5.31$ $\lambda_4 = -5.83$	$\lambda_{5,6} = -5.63 \times 10^{-1} \pm j1.32 \times 10^{1}$	$\lambda_7 \to 0$
15.0	$\lambda_{1,2} = -4.77 \times 10^{-3} \pm j6.97 \times 10^{-2}$	$\lambda_3 = 6.05$ $\lambda_4 = -6.70$	$\lambda_{5,6} = -5.31 \times 10^{-1} \pm j1.26 \times 10^{1}$	$\lambda_7 \to 0$

Table 6 Eigenvalues of Hyperion Flying at Different Speeds and at a height of 85 000 ft

NATURAL MODES OF THE AIRCRAFT				
Height (x103 ft)	**Phugoid**	**Short Period**	**Structural Bending**	**Height**
80	$\lambda_{1,2} = -2.34 \times 10^{-3} \pm j5.99 \times 10^{-2}$	$\lambda_3 = 2.72$ $\lambda_4 = -2.93$	$\lambda_{5,6} = -5.94 \times 10^{-1} \pm j1.60 \times 10^{1}$	$\lambda_7 \to 0$
85	$\lambda_{1,2} = -1.89 \times 10^{-3} \pm j5.78 \times 10^{-2}$	$\lambda_3 = 2.33$ $\lambda_4 = -2.49$	$\lambda_{5,6} = -5.50 \times 10^{-1} \pm j1.64 \times 10^{1}$	$\lambda_7 \to 0$
90	$\lambda_{1,2} = -1.55 \times 10^{-3} \pm j5.24 \times 10^{-2}$	$\lambda_3 = 2.03$ $\lambda_4 = -2.15$	$\lambda_{5,6} = -5.14 \times 10^{-1} \pm j1.68 \times 10^{1}$	$\lambda_7 \to 0$
95	$\lambda_{1,2} = -1.26 \times 10^{-3} \pm j4.53 \times 10^{-2}$	$\lambda_3 = 1.78$ $\lambda_4 = -1.86$	$\lambda_{5,6} = -4.84 \times 10^{-1} \pm j1.70 \times 10^{1}$	$\lambda_7 \to 0$
100	$\lambda_{1,2} = -1.01 \times 10^{-3} \pm j3.91 \times 10^{-2}$	$\lambda_3 = 1.56$ $\lambda_4 = -1.62$	$\lambda_{5,6} = -4.59 \times 10^{-1} \pm j1.72 \times 10^{1}$	$\lambda_7 \to 0$

ity shown by this motion is rapid showing a time constant less than 1 second. Hence, the aircraft longitudinal motion is unstable. Figure 9 shows the response of Hyperion when subjected to a step input change in height. It can be seen here that the aircraft dynamics without any automatic flight control system is unstable.

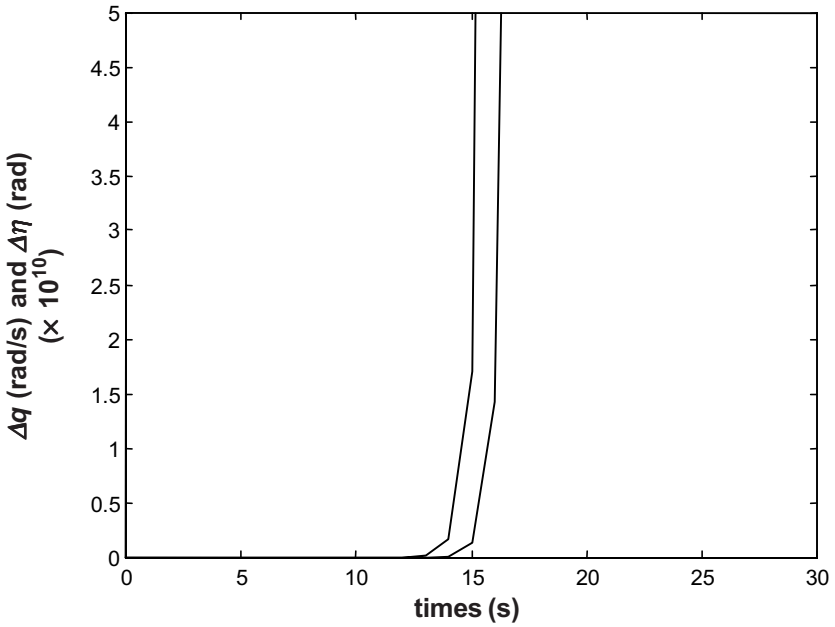

Figure 9 Dynamic responses of Hyperion without any Automatic Flight Control System action

The loci of the aircraft's longitudinal motion eigenvalues have been plotted with respect to changes in vehicle speed and altitude. These eigenvalues were separated into the natural modes of the vehicle viz. its short period mode, phugoid mode, bending mode and height.

Figure 10 shows the short period locus of Hyperion flying at 85 000 ft as its speed is increased. It can be observed that the unstable short period mode becomes increasingly unstable as the speed is increased: the positive real eigenvalues moved further away from the imaginary axis as speed was increased.

The change in the locus of the phugoid mode of the vehicle flying at 85 000 ft is shown in Figure 11. It can be seen that the real parts of the complex eigenvalues moved further from the imaginary axis as speed was increased. Therefore, the phugoid mode became more stable as speed increased. However, the roots were still relatively close to the imaginary axis at the speeds being considered. Note the scale of the real axis. Figure 12 shows the behaviour of the eigenvalues of the bending mode as vehicle speed is increased. From Mach 8.0 to 12.0, the vehicle displayed a set of bending

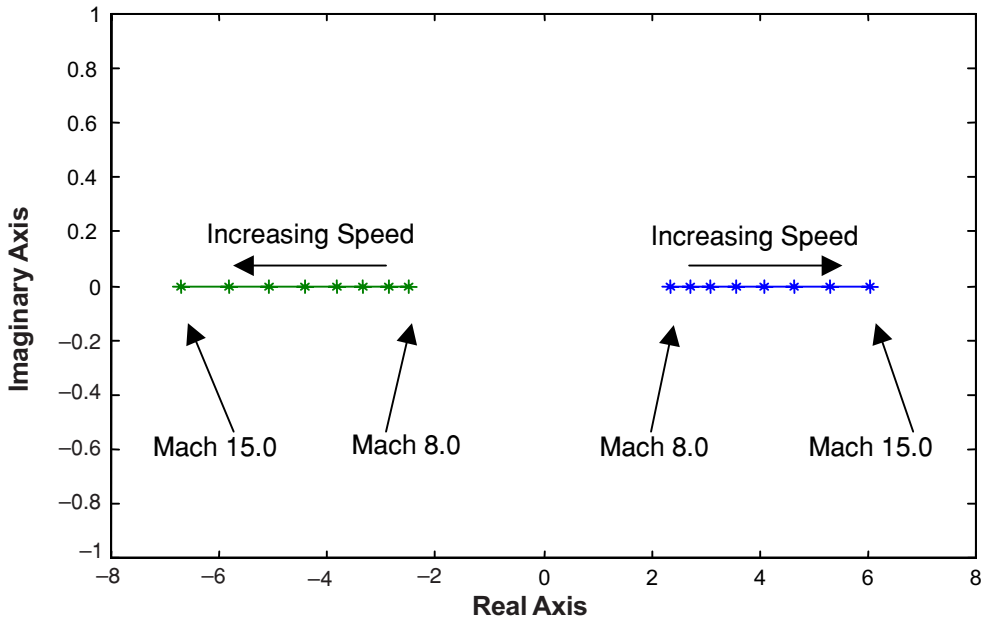

Figure 10 Short Period Mode versus Speed

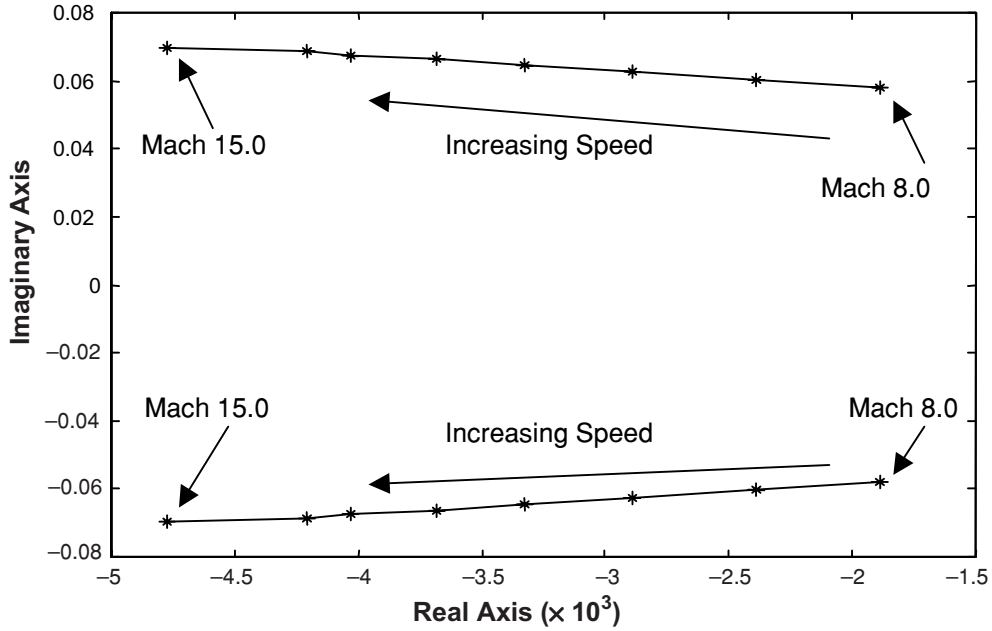

Figure 11 Phugoid Mode versus Speed

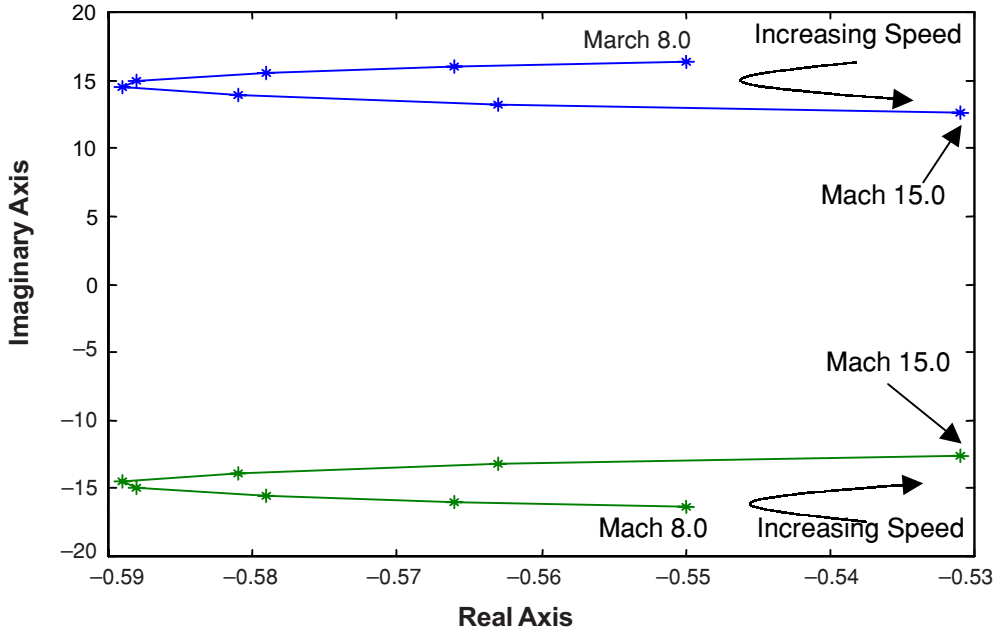

Figure 12 Bending Mode versus Speed

mode eigenvalues which seemed to become more stable because the real part of these eigenvalues moved farther away from the imaginary axis. But the curve turns towards the imaginary axis at speeds Mach 13.0, 14.0 and 15.0. This suggests that the vehicle may tend to become unstable in this bending mode at a higher Mach number.

The natural modes of the vehicle at various heights were analysed next. The vehicle was taken to be flying at Mach 8.0. Figure 13 shows how the short period mode behaved as the vehicle's height was increased: the unstable roots approached the imaginary axis as Hyperion flies higher. At the same time the stable roots approached the imaginary axis in the opposite direction as height increased. The short period mode still remained unstable at these higher altitudes.

Figure 14 shows the phugoid mode eigenvalues as the height of Hyperion increased. Unlike the case for increasing speed, increasing the height of Hyperion results in the phugoid mode approaching instability. Yet at 100 000 ft, Hyperion still displayed a stable phugoid mode.

Similarly, the bending mode seemed to approach instability at higher heights although it remained stable up to 100 000 ft. The eigenvalue for the height mode was virtually zero for every case which implies that the height mode has neutral stability when the vehicle speed and altitude increase.

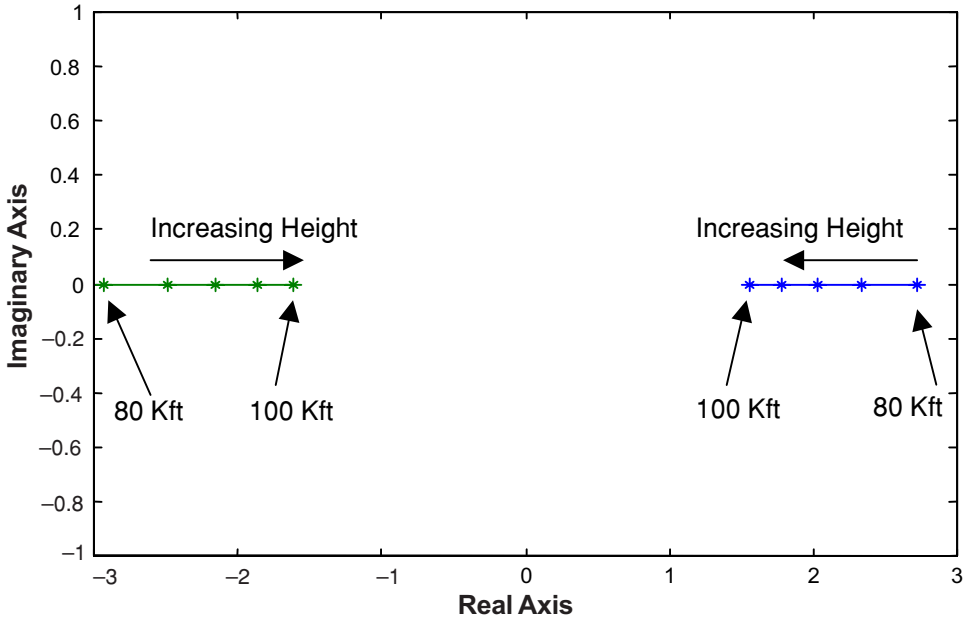

Figure 13 Short Period Mode versus Height

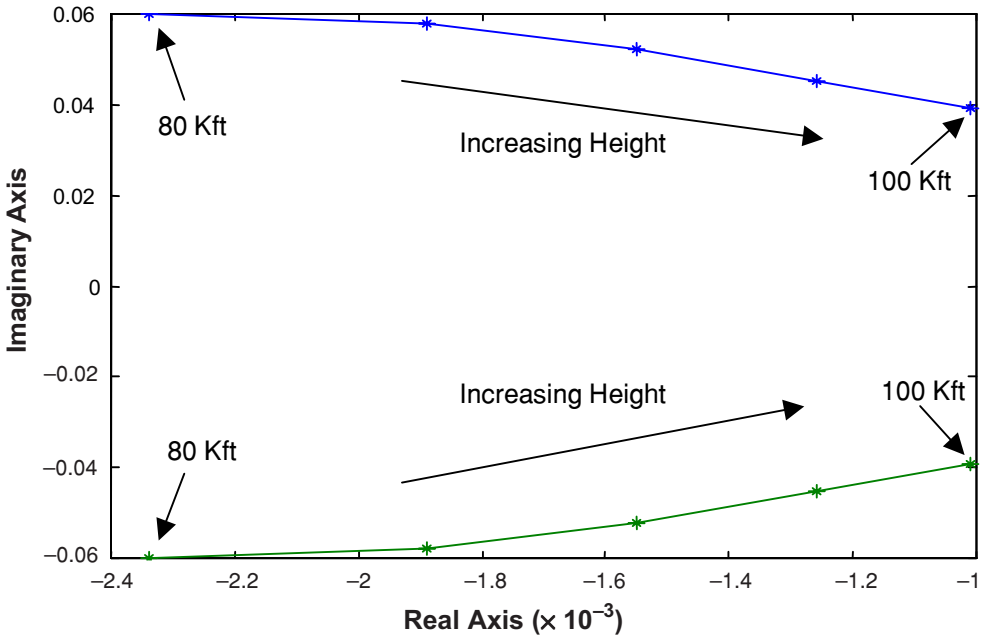

Figure 14 Phugoid Mode versus Height

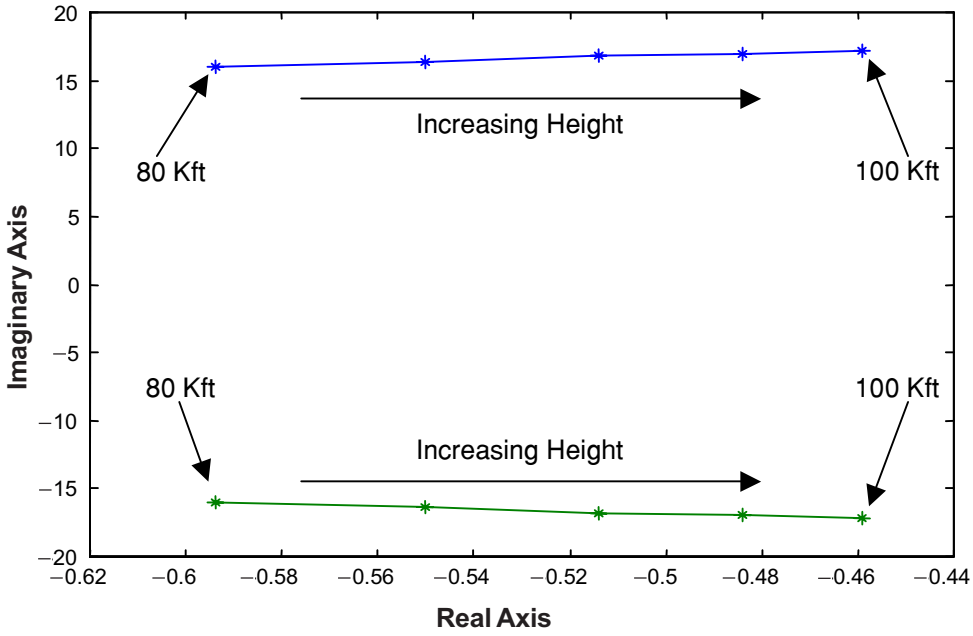

Figure 15 Bending Mode versus Height

8.0 STATIC STABILITY ANALYSIS

The longitudinal static stability of an aircraft can be determined by examining the change in pitching moment due to a change in angle of attack, M_a. [14]. An aircraft is statically stable when $M_a < 0$ *i.e.* any increase in the angle of attack, α, causes an increase in the nose-down pitching moment, thereby tending to reduce the angle of attack. For Hyperion, the changes in the aircraft static stability with respect to speed and altitude are shown in Figure 16.

In addition to the aircraft being dynamically unstable, it can be seen from inspection of M_α that the aircraft is also highly statically unstable. The size of M_α is of the order 106 or higher and in all cases, $M_\alpha > 0$. Note also that when the aircraft was flying at a fixed height of 85 000 ft, increasing speed from Mach 8.0 to 15.0 caused the static stability to deteriorate. However, when the speed of the aircraft was fixed at Mach 8.0 but the height was increased from 80 000 to 100 000 ft, the static stability improved but somewhat was still unstable at 100 000 ft.

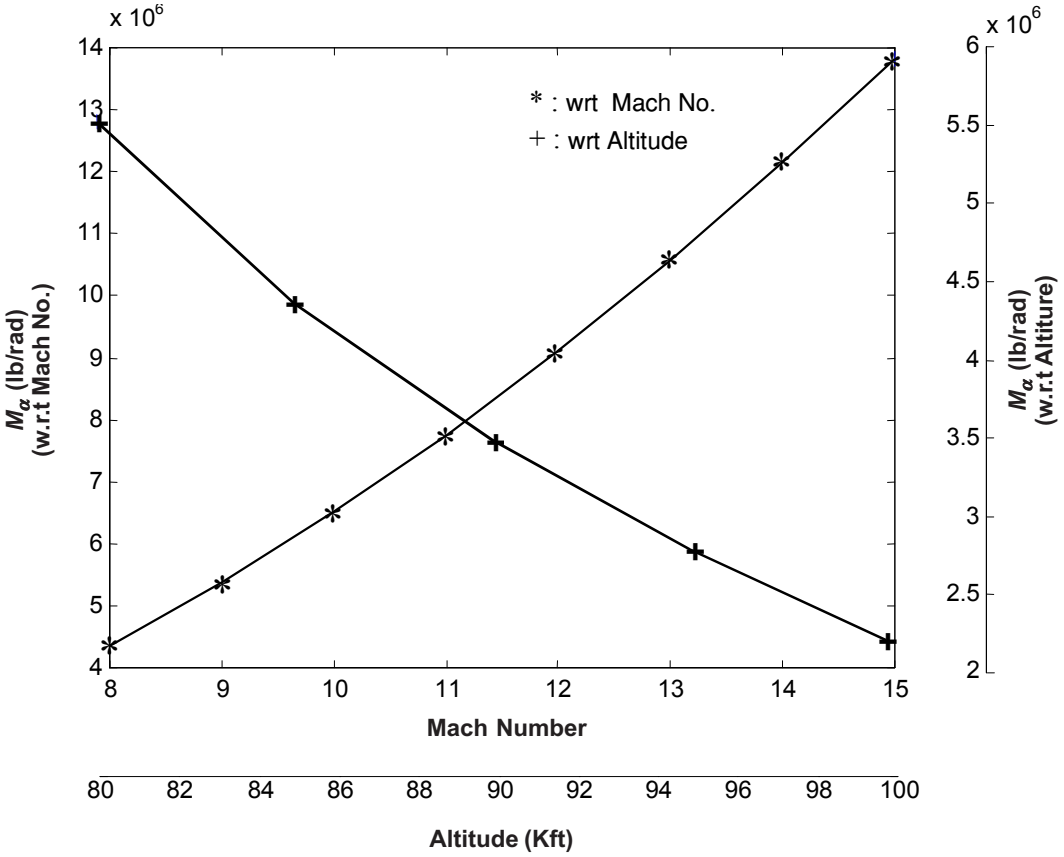

Figure 16 Pitching moment variation with respect to Mach number and height

9.0 CONCLUSIONS

The study of the eigenvalues of the longitudinal motion of the hypersonic transport aircraft without any stability augmentation system has shown that the aircraft becomes progressively less stable at higher Mach numbers and heights. The study of the change in the pitching moment with respect to a change in angle of attack shows that the aircraft static stability deteriorates at higher Mach numbers but improves at higher altitude. Such dynamic characteristics mean that HST aircraft will require effective stability augmentation system if they are to become operational.

ACKNOWLEDGEMENTS

The authors acknowledge the generous financial support of the Universiti Putra Malaysia for the research work on which this paper was based (Research Grant No. 53018).

REFERENCES

[1] Schmidt, D. K. 1996. *Mission Performance, Guidance and Control of a Generic Airbreathing Launch Vehicle*. AAS 96-023, 92: 243-262.

[11] Rogers, G. F. C, and Y. R. Mayhew. 1992. *Thermodynamic and Transport Properties of Fluids - SI Units*. 4th Edition, Oxford: Blackwells.

[2] Beach, H. L., Jr. 1979. Hypersonic Propulsion. *Proceedings of a Conference on Aeropropulsion*. NASA Conference Publication 2092, Lewis Research Center, Cleveland, Ohio, 387-407.

[3] Bowers, A. H., G. K. Noffz, M. Gonda and K. W. Illiff. 1989. A Generic Hypersonic Aerodynamic Model Example (GHAME); *Proposed NASA Technical Memorandum*. AMES Research Centre.

[4] Schmidt, D. K., H. Mamich and F. R Chavez. 1991. Dynamics and Control of Hypersonic Vehicles - The integration Challenge for the 1990's, *AIAA - 91 -5057*, *AIAA Third International Aerospace Planes Conference*. Orlando, Florida.

[5] Bilimore, K. D. and D. K. Schmidt. 1995. An Integrated Development of the Equations of Motion for Elastic Hypersonic Flight Vehicles. *Journal of Control, Guidance and Dynamics.* 18(1): 3-81.

[6] Chavez, F. R, and D. K Schmidt. 1992. An Integrated Analytical Aeropropulsive/Aeroelastic Model for the Dynamic Analysis of Hypersonic Vehicles. *AIAA Paper 92-4567-CP*. AIAA Atmospheric Flight Mechanics Conference, pp 551-563.

[10] Chavez, F. R, and D. K. Schmidt. 1994. Analytical Aeropropulsive/Aeroelastic Hypersonic-Vehicle Model With Dynamic Analysis. *Journal of Guidance, Control and Dynamics*. 17(6): 1308-1319.

[7] Mooij, E. 2001. Numerical Investigation of Model Reference Adaptive Control for Hypersonic Aircraft. *Journal of Guidance, Control and Dynamics*. 24(2): 315-323.

[8] Burken, J. J, P. Lu, Z. Wu, C. Bahm, C. 2001. Two Reconfigurable Flight-Control Design Methods: Robust Servomechanism and Control Allocation. *Journal of Guidance, Control and Dynamics.* 24(3): 482-493.

[9] Lohsoonthorn, P. Jonckheere., E. Daizell, S. 2001. Eigenstructure vs Constrained H(Design for Hypersonic Winged Cone. *Journal of Guidance, Control and Dynamics*. 24(4): 648 - 658.

[12] Zaludin, Z. A. 1998. Mathematical Model of An Aircraft Flying Over a Range of Hypersonic Speeds and Heights, *Technical Report: AASU 98/01*. Aeronautics and Astronautics Department, Southampton University.

[13] Athans, M., and Falb, P. L. 1966. *Optimal Control - An Introduction to the Theory and Its Applications*. McGraw-Hill, NY, pp 149 - 150.

[14] McLean, D. 1993. *Automatic Flight Control System*. Hemel Hempstead, U.K.: Prentice Hall.